Electron Paramagnetic Resonance and Electron Nuclear Double Resonance Study of the Paramagnetic Complexes of Anthraquinone on the Surface of γ-Al2O3

ARTICLE *in* THE JOURNAL OF PHYSICAL CHEMISTRY C · JUNE 2014

Impact Factor: 4.77 · DOI: 10.1021/jp504782y

THE JOURNAL OF PHYSICAL CHEMISTRY C

Article

pubs.acs.org/JPCC

Electron Paramagnetic Resonance and Electron Nuclear Double Resonance Study of the Paramagnetic Complexes of Anthraquinone on the Surface of γ-Al_2O_3

Ildar N. Mukhambetov,[†] Alexander A. Lamberov,[†] Boris V. Yavkin,[‡] Marat R. Gafurov,*[,‡] Georgy V. Mamin,[‡] and Sergei B. Orlinskii[‡]

[†]A. Butlerov Institute of Chemistry of Kazan Federal University, 420008 Kazan, Russia

[‡]EPR Division of Centre of the Shared Facilities of Kazan Federal University, 420008 Kazan, Russia

ABSTRACT: Progress in the synthesis and applications of nanomaterials including nanocatalysts demands a use of precise analytical tools for their surface characterization. Continuous wave (cw) and pulsed electron paramagnetic resonance (EPR) techniques, including electron−nuclear double resonance (ENDOR) have been applied to study paramagnetic complexes formed by adsorption of 9,10-anthraquinone (AQ) as probe molecule by the surface of γ-Al_2O_3. Up to three different paramagnetic complexes (11-line pattern and two single EPR lines) could be separated in our experiments. Their spectroscopic characteristics are extracted. It is shown that at very high concentration (ca. 10 wt %) of AQ, the obtained EPR signal is close to the single line and can be incorrectly interpreted as due to the EPR signal of AQ itself or due to the lower catalytic activity of the investigated surface. That fact should be taken into account by using AQ as a probe of the surface catalytic activity. Mims and Davies ENDOR experiments confirm the redistribution of the electron spin density between the ring protons of AQ, aluminum nuclei in AQ−Al_2O_3 complexes, and remote proton and aluminum nuclei with AQ concentration. The corresponding electron−nuclear distances are extracted. The presented results can be used to expand the application of AQ as a sensitive probe for the catalysts surface characterization.

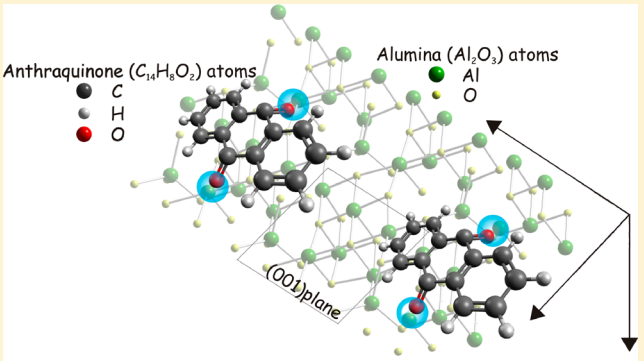

INTRODUCTION

Catalysis is an essential part of many technological developments that have occurred in the past century, and nowadays it plays a central role in the progress of our society. Heterogeneous catalysts promote reactions at the active sites on their surfaces, so they are usually in the form of nanoparticles with a large concentration of active sites. The development of the next generation of (nano)catalysts stands on the shoulders of the surface science techniques that identify and characterize surface active sites at the atomic scale and could be used for the control of the synthesis approaches that are capable of producing stable surface active sites of high concentration.[1,2] Among the most powerful selective methods of the catalysts surface probing the techniques of electron paramagnetic resonance (EPR) and electron−nuclear double resonance (ENDOR) are of particular importance.[3,4] Nowadays they attract a lot of attention for the characterization of nanoscaled materials.[5,6] In this work, taking the paramagnetic complexes of anthraquinone on the surface of γ-Al_2O_3 as model systems, we show some new capabilities and features of the mentioned approaches to qualify the (nano)catalysts surfaces.

The techniques based on the use of paramagnetic spin probes and spin labels are well-known as very efficient tools for investigations of a wide range of objects from the (nano)-material sciences up to the medical applications.[7−11] For the effective use and treatment of the obtained results, the properties of the spin probe (spin label) itself should be well-defined and investigated in details. An illustrative example is nitroxyl radicals with the very complicated temperature, frequency, and concentration dependencies of their EPR spectra.[7,8] Though the properties of nitroxyls are under close study since the 1960s,[12,13] new aspects of their dynamics are to reveal every year that allows getting more information about the systems wherein they are used extending, therefore, the boundaries of their applications.[7−11,14−16] We hope that after some studies, the quinone-based species will occupy their unique place as the probes for the (nano)materials surface characterization, in particular, for the examination of Al_2O_3 surface.

Alumina (aluminum oxide, Al_2O_3) is a low cost material and (in particular, γ-alumina) is the most widely exploited as a catalyst, catalyst support, and adsorbent due to its favorable textural properties and intrinsic acid−base characteristics. Large surface areas, large pore volumes, narrow pore size distributions

Received: May 15, 2014
Revised: June 18, 2014
Published: June 19, 2014

   dx.doi.org/10.1021/jp504782y | J. Phys. Chem. C 2014, 118, 14998−15003

within the mesoporous range, as well as suitable surface acidic−basic properties can often result in favorable enhancements in the catalytic performances. Despite decades of investigations of Al_2O_3 by different analytical methods, the nature of the paramagnetic centers on the material surface is still a matter of the extensive experimental and theoretical studies that open new, sometimes unexpectable horizons of their possible applications.[17,18]

The Lewis acidity of the surface of the alumina is known to arise from coordinatively unsaturated aluminum ions. The strength, concentration, and distribution of such sites are difficult to ascertain, and many techniques have been employed to characterize the surface. 9,10-Anthraquinone (anthraquinone, AQ) is a well-known molecular probe for studying the electron-acceptor and electron-donor properties of oxide catalysts, including aluminosilicates and zeolites.[19−23] This molecule is favorable for the alumina studies because the distance between the two oxygen atoms in the molecular plane is about 0.55 nm, which is close to 0.52 nm between the neighbor aluminum nuclei at the oxide surface. The formation of the AQ complex with two equivalent Al^{3+} cations reveals that the Lewis acid sites are located regularly on the surface of these oxides. Therefore, with help of this method, the concentration of the coordinatively unsaturated aliminium ions could be determined (i.e., the catalytic activity could be quantified and qualified). Nevertheless, the data obtained on the paramagnetic complexes of anthraquinone on catalysts surface remain a subject of controversy, particularly with regard to the mechanism for the formation of paramagnetic complexes and interpretation of the observed EPR spectra.[22]

The application of the pulsed (Fourier-transformed, FT) EPR techniques and pulsed ENDOR to get additional information about the surface sites of Al_2O_3 by exploiting anthraquinone as a magnetic probe and to characterize AQ−Al_2O_3 paramagnetic complexes are presented in this work.

EXPERIMENTAL METHODS

The gamma-alumina was obtained from the high-purity pseudoboehmite (SASOL, Germany) and dried before the treatment at 150 °C for 1 h. Trace components content according to the X-ray fluorescence analysis was SiO_2, Fe_2O_3 < 120 ppm; MgO < 50 ppm; Na_2O, K_2O < 20 ppm; and Ca, Ni, Co, Cr, Pb, Mn, Zn < 100 ppm. Chemically pure 9,10-anthraquinone ($C_{14}H_8O_2$, CAS no. 84-65-1) was provisionally distilled under vacuum.

A glass capillary with the inner diameter of 1.3 mm was filled from one end with the 9.0(1) mg γ-alumina powder with the average sizes of crystallites of 100(50) μm. After that, the end was sealed and the anthraquinone was introduced from the other end in the amounts of 0.1 mg (sample no. 1) or 1 mg (sample no. 2) between the pieces of the fused quartz wool (Horiba: 905.210.660.001). Then, the open end of the capillary was connected to the turbo pump for evacuation, while the alumina-filled part was placed into the furnace and heated up to 500(2) °C with the rate of 20 °C/min. After the degassing during 1 h under the pressure of 10^{-3} Pa, the capillary was sealed from the other end. The product was incubated at 200 °C for 10 h and then cooled down and examined.

Therefore, initial sample of Al_2O_3 (denoted as IS in this work) and samples with low concentration of antraquinone (about 1 wt %, sample no. 1) and high concentration of AQ (about 10 wt %, sample no. 2) were compared in our study.

FT (pulsed) and continuous wave (cw) EPR measurements were done by using X-band (9 GHz) Bruker Elexsys 580 spectrometer equipped with different types of resonators and helium-flow cryostat that allows carrying out the measurements in the temperature range (6−300) K. EPR spectra were recorded by means of standard cw-technique.[24] The external magnetic field $\mathbf{B}_0$ could be swept in the range of 10−1400 mT. Electron spin echo (ESE) detected EPR spectra (which are not shown in this work) were acquired by using a two-pulse echo sequence $\pi/2$-τ-π with the pulse length of $\pi/2$ pulse of 28 ns and time delay τ = 200 ns.

Pulsed ENDOR spectra were detected by Mims sequence $\pi/2$-τ-$\pi/2$-T-$\pi/2$ with an additional radiofrequency (RF) pulse π_{RF} = 16 μs inserted between the second and third microwave $\pi/2$ pulses and Davies sequence π-T-$\pi/2$-τ-π with π_{RF} inserted between the first π pulse and $\pi/2$ pulse.[24,25] RF frequency could be swept in the range of (1−200) MHz.

Because ENDOR is still not too common in most chemical laboratories, some basics of the ENDOR essential for the interpretation of the observed spectra are briefly described below.

In the case of a "free" nucleus, RF pulse applied at the Larmor frequency

$$\nu_{\mathrm{Larmor}} = |\gamma \mathrm{B}_0| \equiv h^{-1}|\mathrm{g}^{(\mathrm{I})}\beta^{(\mathrm{I})}\mathrm{B}_0| \quad (1)$$

where γ is a gyromagnetic ratio of the nuclear spin I, h is a Planck constant, $g^{(I)}$ is a nuclear g-factor, and $\beta^{(I)}$ is a nuclear Bohr magneton; the state of the nuclear spin (the population of the nuclear sublevels) can be changed. In the case of the coupled electron spin S and nuclear spins such changing can modify the state of the electron spin (can change the population of the energy levels contributing to the EPR spectrum). For the hyperfine coupling constant A and simple electron−nuclear coupling (S = 1/2, I = 1/2), it can lead to the appearance of the characteristic features in the ENDOR spectrum at the RF frequencies

$$\nu_{\mathrm{ENDOR}} = \nu_{\mathrm{Larmor}} \pm A/2 \quad (2)$$

or

$$\nu_{\mathrm{ENDOR}} = A/2 \pm \nu_{\mathrm{Larmor}} \quad (3)$$

depending on the ratio between A and ν_{Larmor}.

In polycrystalline media, the ENDOR splitting a_{ENDOR} can help not only identify a type of nuclei coupled with the electron spins but also provide spatial relationships between them. For the first approximation, to estimate the characteristic spatial scale, we assume the pure electron-nuclei dipole−dipole interaction in the point model. In this case, the electron−nuclear distance, r, from the ENDOR splitting can be estimated from

$$a_{\mathrm{ENDOR}} \propto g \cdot g^{(\mathrm{I})}(1 - 3\cos^2\Theta)/r^3 \quad (4)$$

where g is an electronic g-factor, Θ is an angle between and directions of the parallel component of g ($g_{\|}$) and B_0. Though the ENDOR spectra detected in this work are powder spectra, for the rough estimate, we use the "pure" perpendicular orientation. For that the factor $|1 - 3\cos^2\Theta| = 1$.

Simulations of the obtained EPR spectra as well as estimations of the electron-nuclei distances are done using EasySpin toolbox for MatLab.[26]

Other experimental details and examples of some applications of the exploited experimental techniques to study

dx.doi.org/10.1021/jp504782y | J. Phys. Chem. C 2014, 118, 14998−15003

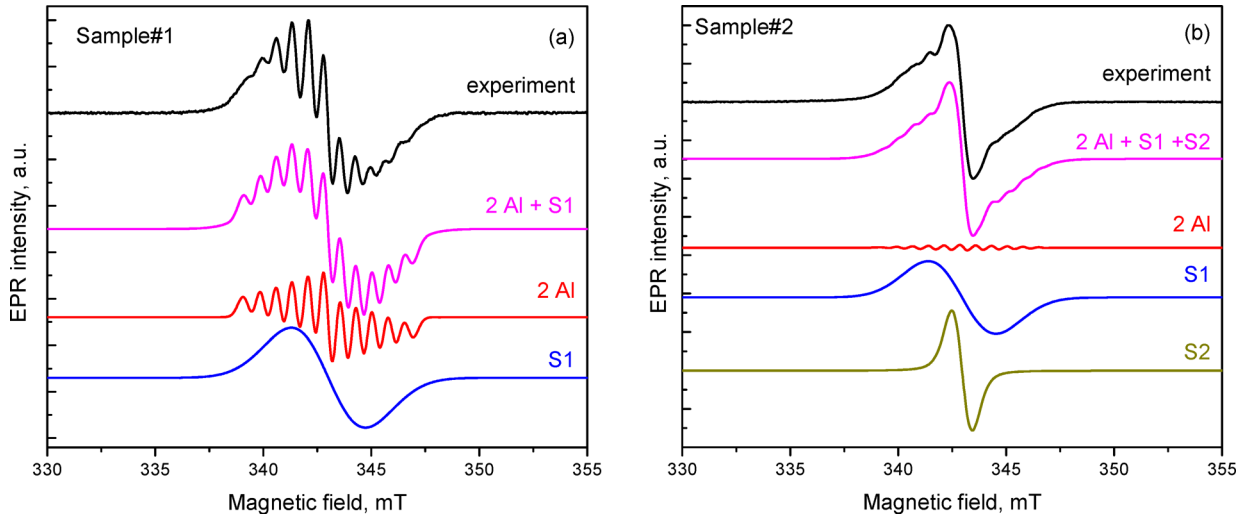

Figure 1. Experimental and simulated cw-EPR spectra of sample nos. (a) 1 and (b) 2 at T = 300 K.

Table 1. Fitting Parameters (Peak-to-Peak Line Width, ΔH_{pp}, g-Factor, Constant of the Hyperfine Interaction, A, and the Statistical Weight) of the Components of the Obtained cw-EPR Spectra Presented on Figure 1[a]

component	S1			S2			2Al			
	ΔH_{pp} (mT)	g-factor	statistical weight	ΔH_{pp} (mT)	g-factor	statistical weight	A (MHz)	ΔH_{pp} (mT)	g- factor	statistical weight
sample no. 1	3.50(10)	2.0040(8)	0.84	–	–	0	20.5(1.2)	0.55(10)	2.0036(8)	0.16
sample no. 2	3.05(10)	2.0040(8)	0.87	0.95	2.0038(8)	0.12	20.5(1.2)	0.48(10)	2.0036(8)	0.01

[a]The uncertainties of the fitting parameters are shown in parentheses.

different matrices and different surface located as well as incorporated paramagnetic complexes could be found in refs 27−29.

RESULTS/DISCUSSION

Though the modern concepts of the surface structure of aluminum oxides are based mainly on the vibrational spectroscopy, and various structural models of the aluminum oxide surface were suggested to explain the experimental data.[30] Our infrared (FT-IR) measurements (Vertex-70, Bruker, Germany) show that FT-IR spectrum of IS is typical for the γ-Al_2O_3 with differently coordinated aluminum. Three spectral regions corresponding to $Al^{IV}OH$ (3780 cm^{-1}), $Al^{VI}(OH)Al^{VI}$ (3740 cm^{-1}), and $Al^{VI}(OH)Al^{IV}$ (3680 cm^{-1}) are the most pronounced for IS in the vicinity of OH vibrational modes. The FT-IR spectra of samples no. 1 and no. 2 are revealed to be the same: a very broad line around 3600 cm^{-1} that corresponds to the hydrogen-bounded hydroxyl groups and two broad peaks about 3550 and 3660 cm^{-1}. Typical solid anthraquinone IR lines at 1580 and 1680 cm^{-1} disappear in the AQ−Al_2O_3 complexes that certify the AQ adsorption for samples nos. 1 and 2.

CW EPR spectra for sample nos. 1 and 2 taken at room temperature along with their simulations are presented in Figure 1 (panels a and b, correspondingly). The lineshapes of the EPR signals do not change with temperature decrease (at least down to T = 20 K), and signal intensities obey the Curie law.

Usually, three paramagnetic centers with practically the same line positions (g-factors) could be obtained in such kind of experiments:[19−21] (1) a six-line pattern due to the paramagnetic complex interacting with a single aluminum ion (a nuclear spin of ^{27}Al with 100% natural abundance is 5/2) that dominates in lithium-modified Al_2O_3, for example, (2) an 11-line spectrum due to the paramagnetic complex interacting with two equivalent aluminum ions, and (3) a single symmetric line which nature is often ascribed to the AQ itself or even not discussed.

EPR spectrum of sample no. 1 could be described satisfactorily as a superposition of an 11-line-containing spectrum (denoted as 2Al) and a single symmetric line (denoted as S1). The second one probably belongs to some additional surface paramagnetic center(s), with the origin still unknown. The simulation parameters are given in Table 1.

To fit the EPR spectrum for sample no. 2, a narrow single line (denoted as S2) to the two described above should be additionally introduced (see Figure 1b and Table 1). Its origin (as well as the origin of the S1 component) is under investigation and is not discussed in detail in this work.

From the first look on the EPR data for sample no. 2 (Figure 1b), an improper conclusion about the lower (in comparison to sample no. 1) catalytic activity of this specimen could be done:[21] the 11-component line 2Al pattern practically disappears. In fact, that is not the case: the only concentration of AQ as a magnetic probe differs in the investigated specimens and a signal of the new paramagnetic center arises.

In attempt to unravel the origin of the obtained surface paramagnetic centers, ENDOR measurements were carried out by using Mims [which is selectively sensitive to the small (super)hyperfine interactions in the system] and Davies (which can give information about the systems with medium to large spin-nuclear interactions)[31] pulse sequences.

Figure 2 presents the Mims and Davies ENDOR spectra detected at T = 20 K in the magnetic field corresponding to the maximal signal of ESE. The four most pronounced symmetrically spaced around the Larmor frequency of ^1H (about 15

dx.doi.org/10.1021/jp504782y | J. Phys. Chem. C 2014, 118, 14998−15003

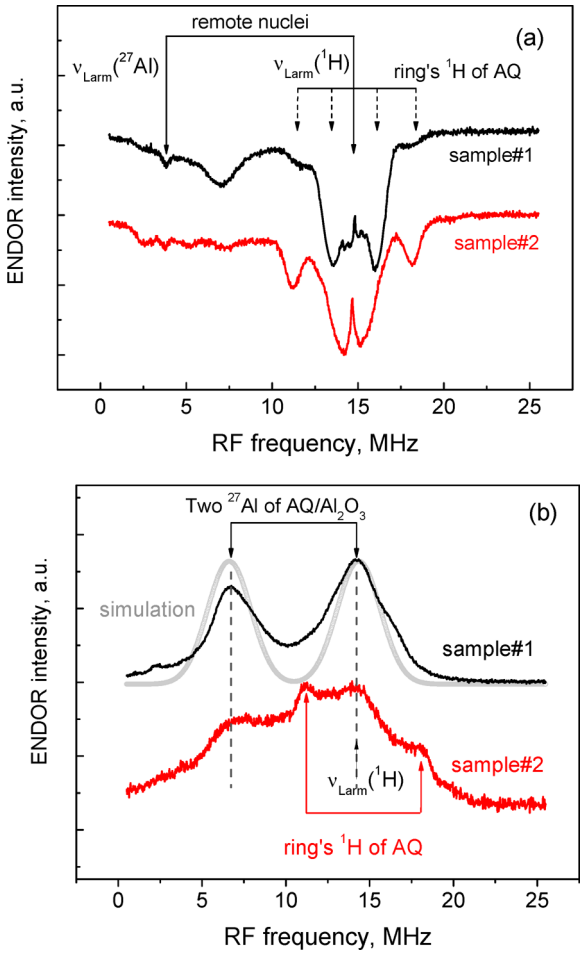

Figure 2. ENDOR spectra for sample nos. 1 and 2 obtained by (a) Mims and (b) Davies pulse sequences at T = 20 K. (a) Spectral features marked with solid arrows coincide with the Larmor frequencies of ^{27}Al and ^{1}H nuclei; dashed arrows refer to the ring's protons of AQ. (b) Spectral features due to the interaction with two equivalent aluminum ions and ring's protons are marked. Noiseless simulation curve (for the well-localized unpaired electron) is shown for ^{27}Al pairs.

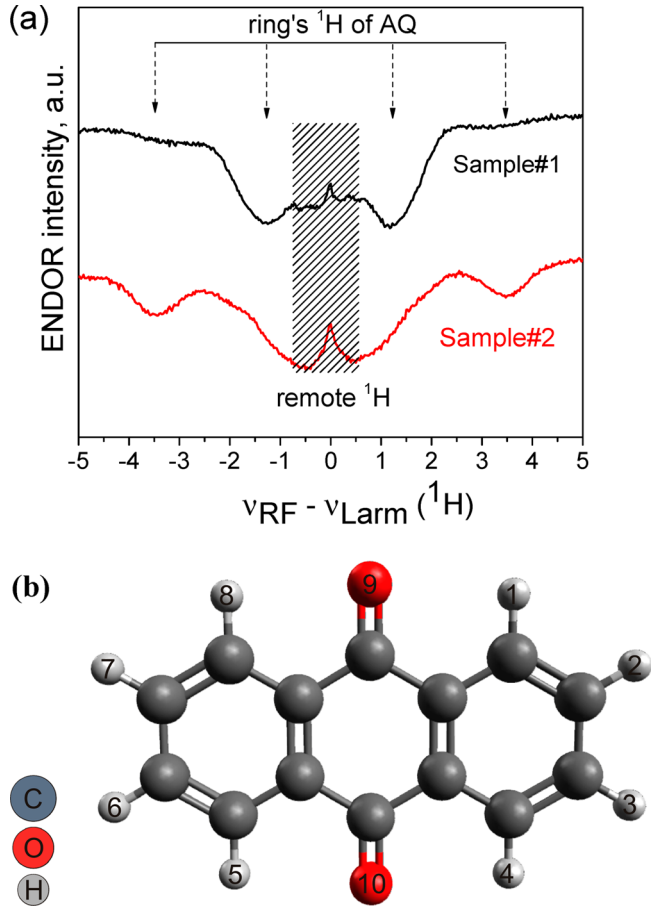

Figure 3. (a) ENDOR spectra of ^{1}H of sample nos. 1 and #2 obtained by Mims pulse sequences at 20 K and (b) schematic representation of the AQ molecule drawn in Avogadro[33] with the marked proton (1−8) and oxygen (9, 10) atoms.

MHz) lines marked in Figure 1a as "ring's ^{1}H of AQ", we ascribe according to eq 2 to the interaction of the unpaired electron with the two pairs of the nonequivalent groups of protons of the aromatic rings of AQ. A more careful examination of the ENDOR spectra of ^{1}H (see Figure 3a) allows defining the parameters of the hyperfine interaction with ^{1}H for sample no. 1 as a_1 = 6.35(15) MHz [0.23(1) mT] and a_2 = 2.45(15) MHz [0.087(6) mT]. The order of the magnitudes of the extracted values is typical for the equivalent pairs of protons in quinone molecules, but their exact values differ from those gathered by A. Fionov.[32] A. Fionov emphasized that these values might reflect the strength of interaction of anthrasemiquinone with the electron-accepting group. Therefore, it could be speculated that potentially the values of a_1 and a_2 extracted from the ENDOR experiments might be used to estimate numerically the strength of the AQ-catalyst surface complexes.

Because the ratio $a_1/a_2 \approx 2.6$ obtained by us is higher than the ratio reported for the components of the hyperfine structures of the AQ complexes [$A_{\|}$ = 4.1, $A_{\perp}$ = 2.5 (i.e., $A_{\|}/A_{\perp}$ = 1.64 for the AQ- γ-Al_2O_3 complexes), see Table 6 in ref 32], we can conclude that a_1 and a_2 are rather isotropic constants for the different pairs of protons. At the present stage of the research, we cannot unambiguously assign the hyperfine splitting constants to the specific proton positions (Figure 3b). We hope that our planned quantum-mechanical calculations and detailed ENDOR studies of a series of differently treated samples can help to clarify this issue.

As followed from the comparison of two curves (Figure 3a), the increase of the probe concentration on the surface of Al_2O_3 leads to the redistribution of the electron spin density between the ring's protons of AQ (cf., the relative intensities of the ENDOR components for the ring's protons in Figure 3a). It gives an opportunity to convert AQ into the sensitive probe for the remote (i.e., not belonging to the AQ molecule) ^{1}H nuclei detection and characterization [a shadowed region around ν_{Larm} (^{1}H) in Figure 3a]. Assuming pure dipole−dipole point−point model of interaction of the unpaired electron with the remote nuclei, from the observed splitting (see eq 4 and explaining that equation text), we can estimate the characteristic probing distance as 0.54 nm for sample no. 1 and 0.44 nm for sample no. 2.

Davies spectra of sample nos. 1 and 2 are the combinations of the ENDOR signals due to the aluminum and hydrogen (Figure 2b). Because for ^{27}Al pairs, the value of A = 20.5 MHz (see Table 1) and Larmor frequency ν_{Larm} (^{27}Al) = 3.83 MHz (in the magnetic field of 345 mT); the aluminum ENDOR patterns in Figure 2b according to eq 3 are centered at $A/2$ and the peaks separated by $2\nu_{Larm}$ (^{27}Al). As can be seen from

dx.doi.org/10.1021/jp504782y | J. Phys. Chem. C 2014, 118, 14998−15003

Figure 2b, the mentioned peaks due to the aluminum pairs also exist in sample no. 2 with the increased AQ concentration on top of the broad intensive ENDOR spectrum. That confirms a presence of aluminum pairs in sample no. 2.

Observation of the symmetrical single line of the finite line width on $\nu_{Larm}(^{27}Al)$ in the Mims ENDOR spectra (Figure 2a) demonstrates that the electron interacts with the remote aluminum nuclei. From that, it can be concluded that the electron wave function extends out of the AQ−2Al complex. From the appearance of the broad ENDOR spectrum for sample no. 2 in the Davies ENDOR pattern (Figure 2b) as in the case of the protons' ENDOR discussed above, a conclusion about the redistribution of the electron spin density and formation of the interface clusters can be done. The clusterization probably leads to the appearance of the narrow (most likely, due to the strong exchange interaction[7−11]) S2 component in the EPR spectrum (Figure 1).

The ENDOR prominences that appear in sample no. 2 and are marked with arrows in Figure 2b are undoubtedly due to the ring's protons with a_1 = 6.35 MHz. To confirm this assumption, we have registered the ENDOR spectra at different values of $\mathbf{B}_0$. Analyzing the spectra, we noted that with $\mathbf{B}_0$ the ENDOR splitting (a_{ENDOR} = 6.35 MHz) did not change while the position of the group center was shifted according to eq 1 proportionally to the protons' gyromagnetic ratio. Additionally, as it is pointed out above, no six-line EPR patterns with the typical hyperfine splitting A_6 = (27−31) MHz[19] were revealed in our EPR spectra. Therefore, we can exclude a hypothetic assignment of the mentioned ENDOR features to the interaction with a single aluminum that might be done due to the closeness of the values of $A_6/2$ and $\nu_{Larm}(^1H)$ in the exploited magnetic fields $\mathbf{B}_0$.

CONCLUSIONS

Some of the obtained in the present work results could be summarized as follows: (1) A new paramagnetic center in AQ−alumina surface complexes arising with the increase of AQ concentration is revealed; (2) ENDOR techniques can be complementary to the EPR information about the existence of aluminum pairs at high AQ concentration; (3) ENDOR techniques could be used for the control of the delocalization of the electron wave function in AQ−Al_2O_3 surface complexes as it appears from the study of ^1H and ^{27}Al ENDOR spectra; (4) changes of the electron wave function density with AQ concentration could be tracked through the changes of ^1H ENDOR spectra.

We realize we are far from full understanding of the properties of AQ−Al_2O_3 surface complexes and the origin of some ENDOR features presented in this work. We hope the results presented in this paper show the fruitfulness of EPR/ENDOR approaches and suppose that after some additional study the quinone-based species will occupy their rightful place as the probes for the (nano)materials surface characterization.

AUTHOR INFORMATION

Corresponding Author

*E-mail: marat.gafurov@kpfu.ru. Tel: +7 843 2926480.

Author Contributions

The manuscript was written through contributions of all authors. All authors have given approval to the final version of the manuscript.

Funding

This work was supported by the Ministry of Education and Science of the Russian Federation, contract no. 02.G25.31.0053. A part of the work is performed according to the Russian Government Program of Competitive Growth of Kazan Federal University. B.V.Y. is grateful to the support of RFBR, research project no. 14−02−31881 mol_a.

Notes

The authors declare no competing financial interest.

REFERENCES

(1) Li, Y.; Somorjai, G. A. Nanoscale Advances in Catalysis and Energy Applications. *Nano Lett.* **2010**, *10*, 2289−2295.

(2) Cargnello, M.; Fornasiero, P.; Gorte, R. J. Playing with Structures at the Nanoscale: Designing Catalysts by Manipulation of Clusters and Nanocrystals as Building Blocks. *Chem. Phys. Chem.* **2013**, *14*, 3869−3877.

(3) Van Doorslaer, S.; Murphy, D. M. EPR Spectroscopy in Catalysis. *Top. Curr. Chem.* **2012**, *321*, 1−39.

(4) Dinse, A.; Wolfram, T.; Carrero, C.; Schlögl, R.; Schomäcker, R.; Dinse, K.-P. Exploring the Structure of Paramagnetic Centers in SBA-15 Supported Vanadia Catalysts with Pulsed One- and Two-Dimensional Electron Paramagnetic Resonance (EPR) and Electron Nuclear Double Resonance (ENDOR). *J. Phys. Chem. C* **2013**, *117*, 16921−16932.

(5) Baranov, P. G.; Orlinskii, S. B.; de Mello Donegá, C.; Schmidt, J. High-Frequency EPR, ESE, and ENDOR Spectroscopy of Co- and Mn-Doped ZnO Quantum Dots. *Phys. Status Solidi B* **2013**, *250*, 2137−2140.

(6) Baranov, P. G.; Orlinskii, S. B.; de Mello Donegá, C.; Schmidt, J. High-Frequency EPR and ENDOR Spectroscopy on Semiconductor Quantum Dots. *Appl. Magn. Reson.* **2010**, *39*, 151−183.

(7) Eaton, S. S.; Eaton, G. R.; Berliner, L. J. *Biomedical EPR - Part A: Free Radicals, Metals, Medicine and Physiology*; Springer: New York, 2005.

(8) Kokorin, A. I. *Nitroxides - Theory, Experiment and Applications*; InTech: Rijeka, 2012, DOI: 10.5772/2887.

(9) Nagasaki, Y. Nitroxide Radicals and Nanoparticles: a Partnership for Nanomedicine Radical Delivery. *Ther. Delivery* **2012**, *3*, 165−179.

(10) Burlaka, A. P.; Ganusevich, I. I.; Gafurov, M. R.; Lukin, S. N.; Sidorik, E. P. Electron Paramagnetic Resonance Study of Tumor Affected Bone Marrow. *Cancer Microenviron.* **2013**, *6*, 273−276.

(11) Burlaka, A.; Selyuk, M.; Gafurov, M.; Lukin, S.; Potasaklova, V.; Sidorik, E. Changes in Mitochondrial Functioning with Electromagnetic Radiation of Ultra High Frequency as Revealed by Electron Paramagnetic Resonance Methods. *Int. J. Radiat. Biol.* **2014**, *90*, 357−362.

(12) Axel, F. S. Biophysics with Nitroxyl Radicals. *Biophys. Struct. Mech.* **1976**, *2*, 181−218.

(13) Buchachenko, A. L.; Wasserman, A. M. *Stable Radicals. Electronic Structure, Reactivity and Application*; Khimiya: Moscow, 1973 (in Russian).

(14) Gafurov, M.; Denysenkov, V.; Prandolini, M. J.; Prisner, T. Temperature Dependence of the Proton Overhauser DNP Enhancements on Aqueous Solutions of Fremy's Salt Measured in a Magnetic Field of 9.2 T. *Appl. Magn. Reson.* **2012**, *43*, 119−128.

(15) Gafurov, M. R. TEMPOL as a Polarizing Agent for Dynamic Nuclear Polarization of Aqueous Solutions. *Magn. Reson. Solids* **2013**, *15*, 13103.

(16) Orlinskii, S. B.; Borovykh, I. V.; Zielke, V.; Steinhoff, H.-J. Use of Spin Labels to Study Membrane Proteins by High-Frequency Electron Nuclear Double Resonance Spectroscopy. *JETP Lett.* **2007**, *86*, 149−152.

(17) Trueba, M.; Trasatti, S. P. γ-Alumina as a Support for Catalysts: A Review of Fundamental Aspects. *Eur. J. Inorg. Chem.* **2005**, *17*, 3393−3403.

(18) Lee, D.; DuBois, J. L.; Lordi, V. Identification of the Local Sources of Paramagnetic Noise in Superconducting Qubit Devices

Fabricated on α-Al_2O_3 Substrates Using Density-Functional Calculations. *Phys. Rev. Lett.* **2014**, *112*, 017001.
(19) Lunina, E. V.; Markaryan, G. L.; Fionov, A. V.; Astashkin, A. V.; Samoilova, R. I.; Zdravkova, M. T. ENDOR Study of Anthraquinone Paramagnetic Complexes with Lewis Acid Centers of Aluminium Oxide. *Appl. Magn. Reson.* **1991**, *2*, 675−681.
(20) Samoilova, R. I.; Dikanov, S. A.; Fionov, A. V.; Tyryshkin, A. M.; Lunina, E. V.; Bowman, M. K. Pulsed EPR Study of Orthophosphoric and Boric Acid Modified Gamma-Alumina. *J. Phys. Chem.* **1996**, *100*, 17621−17629.
(21) Samoilova, R. I.; Moroz, E. M.; Lund, A.; Tsvetkov, Y. D. Surface Properties of Alumnas as Studied by the Electron-Nuclear Double Resonance Method. *Russ. J. Phys. Chem. A* **2001**, *75*, 629−635.
(22) Fionov, V.; Nekhaev, A. I.; Shchapin, I.Yu.; Maksimov, A. L.; Lunin, V. V. Paramagnetic Complexes of 9,10-Anthraquinone on Zeolite Surfaces and Their Thermal Transformations. *Russ. J. Phys. Chem. A* **2013**, *87*, 1947−1951.
(23) Lunina, E. V.; Zacharova, M. N.; Markaryan, G. L.; Fionov, A. V. The Application of Paramagnetic Complexes of Probe Molecules for the Investigation of the Lewis Acidity of Aluminas. *Colloids Surf., A* **1996**, *115*, 195−206.
(24) Weil, J. A.; Bolton, J. R. *Electron Paramagnetic Resonance: Elementary Theory and Practical Applications*, 2nd ed.; John Wiley & Sons: Hoboken, NJ, 2004.
(25) Murphy, D. M.; Farley, R. D. Principles and Applications of ENDOR Spectroscopy for Structure Determination in Solution and Disordered Matrices. *Chem. Soc. Rev.* **2006**, *35*, 249−268.
(26) Stoll, S.; Schweiger, A. EasySpin, a Comprehensive Software Package for Spectral Simulation and Analysis in EPR. *J. Magn. Reson.* **2006**, *178*, 42−55.
(27) Yavkin, B. V.; Mamin, G. V.; Orlinskii, S. B.; Gafurov, M. R.; Salakhov, M. Kh.; Biktagirov, T. B.; Klimashina, E. S.; Putlayev, V. I.; Tretyakov, Yu. D.; Silkin, N. I. Pb^{3+} Radiation Defects in $Ca_9Pb(PO_4)_6(OH)_2$ Hydroxyapatite Nanoparticles Studied by High-Field (W-band) EPR and ENDOR. *Phys. Chem. Chem. Phys.* **2012**, *14*, 2246−2249.
(28) Gafurov, M.; Biktagirov, T.; Yavkin, B.; Mamin, G.; Filippov, Y.; Klimashina, E.; Putlayev, V.; Orlinskii, S. Nitrogen-Containing Species in the Structure of the Synthesized Nano-Hydroxyapatite. *JETP Lett.* **2014**, *99*, 196−203.
(29) Biktagirov, T.; Gafurov, M.; Mamin, G.; Klimashina, E.; Putlayev, V.; Orlinskii, S. Combination of EPR Measurements and DFT Calculations to Study Nitrate Impurities in the Carbonated Nanohydroxyapatite. *J. Phys. Chem. A* **2014**, *118*, 1519−1526.
(30) Belskaya, O.; Danilova, I.; Kazakov, M.; Mironenko, R.; Lavrenov, A.; Likholobov. V. FTIR Spectroscopy of Adsorbed Probe Molecules for Analyzing the Surface Properties of Supported Pt (Pd) Catalysts. In *Infrared Spectroscopy - Materials Science, Engineering and Technology*; Theophile, T., Ed.; InTech: Rijeka, 2012, DOI: 10.5772/36275.
(31) Goldfarb, D.; Arieli, D. Spin Distribution and the Location of Protons in Paramagnetic Proteins. *Annu. Rev. Biophys. Biomol. Struct.* **2004**, *33*, 441−468.
(32) Fionov, A. V. Paramagnetic Complexes of 9,10-Anthraquinone and 9-Fluorenone on the Metal Oxide Surface. *Russ. Chem. Bull.* **2009**, *58*, 538−550.
(33) Hanwell, M. D.; Curtis, D. E.; Lonie, D. C.; Vandermeersch, T.; Zurek, E.; Hutchison, G. R. Avogadro: An Advanced Semantic Chemical Editor, Visualization, and Analysis Platform. *J. Cheminf.* **2012**, *4*, 17.